Materials Today Communications, Volume 46, June 2025, Article number 112655
DOI:10.1016/j.mtcomm.2025.112655

# Effect of the combined use of cryogenic+ aging treatment on mechanical and damping property of Mn-Cu alloy based on response surface model

*Ding Ran[1,2], Liu Guang-lei[1], Liu Shu-cong[1], Mostafa Ranjbar[2], Andrew Potter[2], Liu Hai-xia[1], Lu Bin[3], lubin@jstqie.com Ji Jian-fei[3] jijianfei@jstqie.com*

1. School of Materials Science and Engineering, Jiangsu University, Zhenjiang 212013

2. Cranfield university

3. Jiangsu Tianqi New Material Application Research Institute Co., Zhenjiang 212009

**ABSTRACT** In this paper, Response Surface Methodology (RSM) is used to model the response surface between the target values and the cryogenic + aging treatment parameters. Then the effects of cryogenic + aging treatment on microstructures, mechanical, and damping properties of M2052 were investigated. The outcome indicated cryogenic + aging compound treatment can effectively enhance both mechanical and damping properties, and the optimum parameters cryogenic(-196℃/30h) + aging(428℃/2h) were obtained. The associated microstructural changes caused by the precipitated phase after compound treatment resulted in an increase in tensile strength from 358.3 MPa to 396.7 MPa, ~38MPa higher compared to the as-cast alloy. Meanwhile, it has the best damping property within a wider temperature range. At 50℃, the internal friction value increased from 0.033 to 0.074, which was increased by 124%. The damping strengthening mechanisms were discussed mainly from the perspective of the change in formation of {101} twins and motionable interface induced by fcc-fct transformation after compound treatment. The results in this paper provide a new reference for simultaneously improving mechanical and damping behaviors of Mn-Cu based alloys.

**KEY WORDS**：Mn-Cu damping alloy；Cryogenic and aging treatment；Response surface method；mechanical property; damping capacity

## 1 Introduction

Engineering structures in the field of high-precision parts and vehicle transportation face the problem of mechanical vibration under external forces, which will greatly affect the service and safety performance of machinery and equipment [1-3]. The damping properties can transform mechanical vibration energy into thermal energy, thus effectively reducing the mechanical vibration [4]. As a representative twin-type high damping MnCu based alloy, M2052 has received much attention because of its extraordinary damping capacity and excellent mechanical properties [5-6]. The damping property of M2052 alloy is closely related to the martensite structure. Owing to the movement between different martensitic interfaces, austenitic and martensitic interfaces, as well as twin interfaces can dissipate energy [7-9]. The hysteresis motion of defects and dislocations also contributes to part of energy dissipation, thus effectively reducing the mechanical vibration of materials [4,10-11].

As we all know, the mechanical and damping behaviors of most alloys usually display inverse trends, which makes it a great challenge to simultaneously enhance the mechanical and damping properties [12-14]. Aging treatment has been verified as an effective way to obtain precipitated phases that can significantly change the microstructure and comprehensive properties of the alloy [15-17]. During aging treatment, spinodal decomposition occurs and Mn-rich and Cu-rich regions form. Accordingly, an antiferromagnetic transition and subsequent fcc-fct



Published by Elsevier. This is the Author Accepted Manuscript issued with: Creative Commons Attribution License (CC:BY 4.0).
The final published version (version of record) is available online at DOI:10.1016/j.mtcomm.2025.112655. Please refer to any applicable publisher terms of use.

martensitic transformation take place in the Mn-rich regions, leading to the formation of twins which contribute to the high damping capacity [18-21]. Wang et al. [22] showed that the damping performance can be improved efficiently in ZMD-1J MnCu alloys after aging at 430℃ for 2 hours. Li et al. [23] showed that step-cooling after aging treatment can significantly improve the damping capacity of M2052 alloy. Alloying is the simplest and most direct way to change grain size [24-28]. Yin et al. proposed that Ni addition in Mn-Cu alloy obviously increases the damping capacity, while the transformation temperature of the Ni added alloy is decreased by the retarded phase decomposition of γ Mn phase [29]. Different processing and preparation technologies were applied to preparing Mn-Cu alloy aims to enhance the damping capability. Wang et al. reported that the directionally solidified MnCu alloy prepared under high magnetic field owns high damping capacity in a wide temperature range from 200K to 320K [30]. Li et al. shows that novel Mn-Cu porous materials prepared by the powder metallurgy exhibit high damping capacity [31]. In fact, previous investigations on MnCu based alloy have primarily focused on aging, solid solution, solid solution+aging, alloying, etc processes. However, the damping capacity of the alloy mostly can be obtained only in the temperature range below room temperature. Therefore, for the actual needs of engineering, exploring how to enhance comprehensive performance within a wide temperature range for MnCu based alloy has become quite urgent.

Cryogenic treatment is a process method in which liquid nitrogen is used as the cooling medium to make the material be treated in an ultra-low temperature environment at -196℃ [32]. Cryogenic treatment can improve the mechanical properties of the material by promoting the decomposition of unstable phase, refining grain, increasing dislocation density and inducing twins [33]. Cryogenic treatment is often used as a supplement to heat treatment, and combined with the traditional heat treatment process, it has different effects on material properties [34]. However, the influence of compound treatment (cryogenic+aging) on the microstructure, mechanical property and damping capacity of MnCu based alloy has not been systematically investigated. Therefore, in this paper, impacts of the interaction between compound treatment (Cryogenic treatment +aging) on the mechanical property for M2052 alloy was studied using response surface method (RSM), and the microstructure and damping capacity of the sample treated under different cryogenic treatment +aging parameters were studied.

## 2 Experimental

The raw material is as-cast M2052 alloy produced by TianQi company, and the chemical composition is shown in Table 1. The specimens were cryogenic treated in liquid nitrogen tank followed by aging treatment conducted in DZF-6020AB drying oven. Specifically, the temperature of cryogenic treatment is -196℃, and the holding time range is 6h-36h. The aging temperature range is 350-500℃ with soaking time range of 2h-10h. After aging treatment was completed, the specimens were removed from the drying oven followed by air cooling.

Table 1 The chemical compositions of the raw material M2052 alloy (mass%)

| Element | Si | P | Cu | Ni | Fe | C | S | Mn |
|---|---|---|---|---|---|---|---|---|
| Mass fraction% | 0.017 | ＜0.05 | 20.03 | 4.83 | 1.96 | 0.0049 | 0.02 | Bal. |

### 2.1 Phase and microstructure characterization

The microstructure of specimens was observed by a German Zeiss metallographic microscope (OM). The distribution of elements in different regions was analyzed using an energy-dispersive analyzer (EDS) accessory of an American FEI Nova Nano 450 scanning electron microscope (SEM). The interface microstructure, crystallographic orientation and orientation were investigated via electron backscatter diffraction (EBSD) at field emission scanning electron microscope (FE-SEM). Phase identification was carried out by the X-ray diffractometer (XRD, D8 Advance) with a Cu Kα radiation and a step size of 0.02°.

### 2.2 Mechanical and damping properties characterization

Tensile strength performed by universal testing machine (MTS-DDL100) at 1mm/min according to test standard GB/ T 228. 1-2021. The tensile test specimens were designed as flat type with dimension of 62×14×2 mm. The damping capacity, loss tangent (tanδ) was obtained through dynamical mechanical analyzer (DMA) (Q800) with specimen dimension size of 2mm*8mm*35mm. The heating rate is 5℃ /min, and the test temperature range was-100℃–200 ℃with a frequency of 10 Hz and strain amplitude of $5*10^{-4}$.

## 3 Results and Discussion

### 3.1 Experimental design and results of RSM

In this study, aging time(t), aging temperature (T) and cryogenic time (P) were selected as the most important parameters for controlling the cryogenic + aging treatment process. A Box–Behnken design (BBD) was employed to establish a total of 17 test schemes with 3 center points. Ultimate strength and elongation were utilized to represent the mechanical properties of the material. Table 2 shows the specific design scheme and test results.

Table 2 Experimental design and analysis results of response surface method

| Experiment No. | Parameter | | | Response | |
|---|---|---|---|---|---|
| | t/h | T/℃ | P/h | Rm/MPa | A/% |
| 1 | 6 | 350 | 6 | 350.0 | 30.2 |
| 2 | 6 | 425 | 21 | 404.7 | 29.8 |
| 3 | 10 | 425 | 36 | 417.3 | 27.4 |
| 4 | 2 | 425 | 36 | 398.8 | 31.9 |
| 5 | 6 | 500 | 36 | 356.2 | 32.0 |
| 6 | 6 | 350 | 36 | 369.3 | 32.0 |
| 7 | 6 | 425 | 21 | 404.8 | 29.4 |
| 8 | 2 | 350 | 21 | 363.8 | 34.3 |
| 9 | 2 | 425 | 6 | 373.5 | 30.1 |
| 10 | 10 | 500 | 21 | 376.5 | 30.6 |
| 11 | 2 | 500 | 21 | 340.9 | 37.9 |
| 12 | 10 | 425 | 6 | 411.7 | 26.3 |
| 13 | 10 | 350 | 21 | 377.0 | 31.8 |
| 14 | 6 | 500 | 6 | 350.4 | 31.8 |
| 15 | 6 | 425 | 21 | 399.4 | 29.1 |
| 16 | 6 | 425 | 21 | 401.2 | 29.4 |
| 17 | 6 | 425 | 21 | 402.3 | 29.5 |

### 3.2 Response surface modeling

Table 3 shows the results for the variance analysis of the ultimate strength. The F-value of the ultimate strength prediction model is 154.42, indicating that the model is significant. In the table, df represents the degree of freedom, F-value and P-value are the results obtained from the significance test of the model and the coefficient of the model in the analysis of variance, PC represents the sum of squares of each model in the percentage of the total square. A P value of less than 0.05 indicates that the item in the model is significant; hence, the aging time (t), aging temperature (T), cryogenic time (P), interaction items tT, tP, and TP, and quadratic items $t^2$, $T^2$, $P^2$ are significant. $R^2$ is 0.995, indicating that the experimental value is highly correlated with the predicted value. The significance, model coefficients, and missing items of the response model were tested, and the best fitting model was selected on the basis of the fitting analysis. Stepwise regression was adopted to screen and eliminate the insignificant items in the model. Adjusted $R^2$and predicted $R^2$ are 0.9885 and 0.9523, respectively, with a difference of less than 0.2. The Adeq signal-to-noise ratio is 37.1098 and greater than 4, verifying that the model is reliable and that the model can

be used for improving the experimental design.

Table 3 Variance analysis results of ultimate strength

| Source | Sum of squares | df | Mean square | F value | P value | Significance<0.05 |
|---|---|---|---|---|---|---|
| Model | 9484.04 | 9 | 1053.78 | 154.42 | <0.0001 | Significant |
| t | 1392.1 | 1 | 1392.1 | 203.99 | <0.0001 | Significant |
| T | 162.4 | 1 | 162.4 | 23.8 | 0.0018 | Significant |
| P | 390.78 | 1 | 390.78 | 57.26 | 0.0001 | Significant |
| tT | 124.74 | 1 | 124.74 | 18.28 | 0.0037 | Significant |
| tP | 97.22 | 1 | 97.22 | 14.25 | 0.0069 | Significant |
| TP | 46.03 | 1 | 46.03 | 6.74 | 0.00356 | Significant |
| $t^2$ | 37.85 | 1 | 37.85 | 5.55 | 0.0507 | Insignificant |
| $T^2$ | 7048.2 | 1 | 7048.2 | 1032.82 | <0.0001 | Significant |
| $P^2$ | 109.24 | 1 | 109.24 | 16.01 | 0.0052 | Significant |
| Residual | 47.77 | 7 | 6.82 | | | |
| Lack of fit | 26.34 | 3 | 8.78 | 1.64 | 0.3151 | Insignificant |
| Pure error | 21.43 | 4 | 5.36 | | | |
| Cor total | 9531.81 | 16 | | | | |
| Std. Dev. | 2.61 | | $R^2$ | 0.995 | | |
| Mean | 382.2 | | Adjusted $R^2$ | 0.9885 | | |
| C.V.% | 0.6835 | | Predicted $R^2$ | 0.9523 | | |
| | | | Adeq Precision | 37.1098 | | |

Table 4 Variance analysis results of elongation

| Source | Sum of squares | df | Mean square | F value | P value | Significance<0.05 |
|---|---|---|---|---|---|---|
| Model | 110.5 | 9 | 12.28 | 118.99 | <0.0001 | Significant |
| t | 40.86 | 1 | 40.86 | 395.98 | <0.0001 | Significant |
| T | 1.96 | 1 | 1.96 | 19 | 0.0033 | Significant |
| P | 3.03 | 1 | 3.03 | 29.32 | 0.001 | Significant |
| tT | 5.66 | 1 | 5.66 | 54.89 | 0.0001 | Significant |
| tP | 0.1764 | 1 | 0.1764 | 1.71 | 0.2324 | Insignificant |
| TP | 0.64 | 1 | 0.64 | 6.2 | 0.0416 | Significant |
| $t^2$ | 2.81 | 1 | 2.81 | 27.24 | 0.0012 | Significant |
| $T^2$ | 48.87 | 1 | 48.87 | 473.64 | <0.0001 | Significant |
| $P^2$ | 7.48 | 1 | 7.48 | 72.5 | <0.0001 | Significant |
| Residual | 0.7223 | 7 | 0.1032 | | | |
| Lack of fit | 0.4668 | 3 | 0.1556 | 2.44 | 0.2048 | Insignificant |
| Pure error | 0.2555 | 4 | 0.0639 | | | |
| Cor total | 111.22 | 16 | | | | |
| Std. Dev. | 0.3212 | | $R^2$ | 0.9935 | | |
| Mean | 30.79 | | Adjusted $R^2$ | 0.9852 | | |
| C.V.% | 1.04 | | Predicted $R^2$ | 0.9293 | | |
| | | | Adeq Precision | 46.0685 | | |

The same method was adopted to optimize and analyze the elongation model. Table 4 shows the corresponding variance analysis results of elongation. The mathematical model of ultimate strength and elongation with process parameters is established as follows.

$R_m$= −908.42365−5.13644 t+6.07411 T+3.19127 P+0.018614 tT−0.082167 tP−0.003015 TP+0.187397 $t^2$−

$0.007274\ T^2 - 0.022638\ P^2$ (1)

$A = 124.04879 + 0.581583\ t - 0.476969\ T + 0.461938\ P - 0.003967\ tT - 0.003500\ tP - 0.000356\ TP + 0.051062\ t^2 + 0.000606\ T^2 - 0.005924\ P^2$ (2)

Where: $R_m$ is the ultimate strength (MPa), A is the elongation, t is aging time (h), T is the aging temperature (℃), P is the cryogenic time (h).

Fig. 1 shows the normal distribution of residuals and the comparison between the predicted and experimental values of ultimate and elongation. The residual values of each response prediction model are linearly distributed, and the residual value exhibits a uniform distribution, indicating that the model is self-adaptive (Fig. 1(a) and (c)). Each response model exhibits a high prediction accuracy (Fig. 1(b) and (d)).

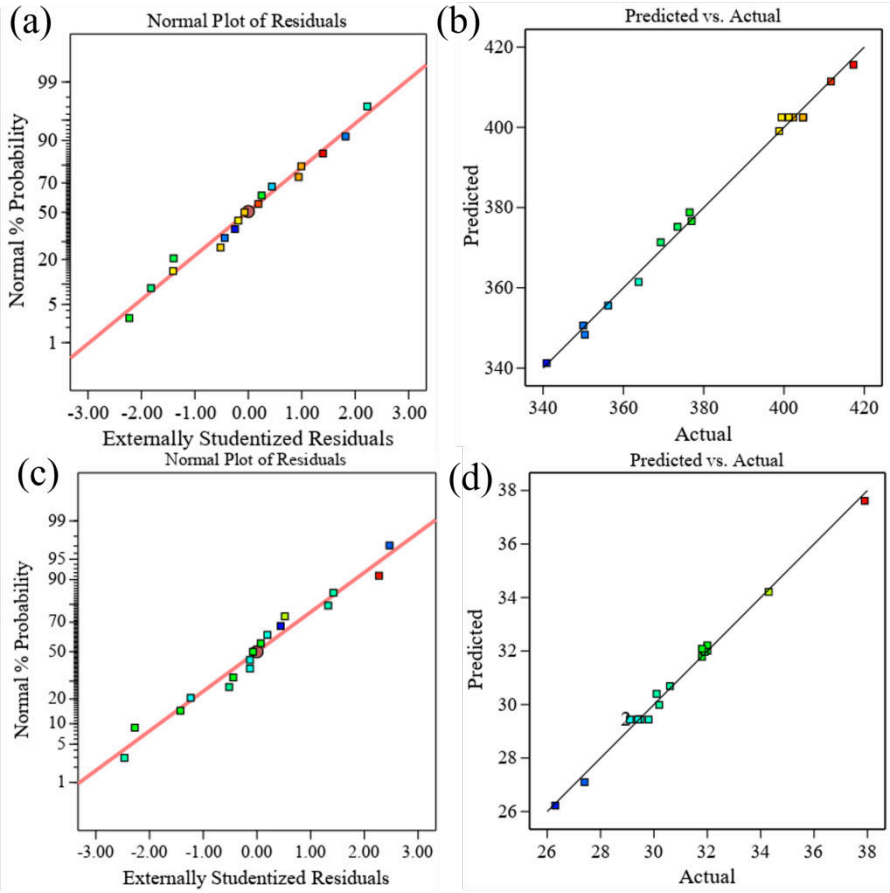


Fig. 1 Residual normal distribution and prediction-actual distribution: (a) and (b) are ultimate strength; (c) and (d) are elongation

### 3.3 Analysis of the effect of process parameter interactions on response values

Effects of interactions among process parameters on the ultimate strength were manifested by 3D surface response and contour lines, as shown in Fig.2. Fig.2(a-b) shows the response surface of the interaction influence of aging temperature and aging time on the ultimate strength. The curvature of the surface is obvious, and the curvature change in the B direction is larger than that in the A direction, indicating that the aging temperature has a greater influence on the ultimate strength in the interaction between aging temperature and time. With aging temperature increases, the ultimate strength increases firstly then decreases. The ultimate strength increases with aging time increase. The response surface of the interaction between cryogenic time and aging time against tensile strength is shown in Figure 2 (c-d). The tensile strength of the alloy is lower when the cryogenic time and aging time are shorter. With the extension of cryogenic time and aging time, the tensile strength of the alloy will keep rising. The interaction between cryogenic time and aging temperature is shown in Figure 2 (e-f). As the aging temperature increases, the tensile strength increases first and then decreases. After the addition of cryogenic treatment, although the effect of

aging temperature on tensile strength is not changed, extending cryogenic time at the same aging temperature can further improve the tensile strength of the alloy.

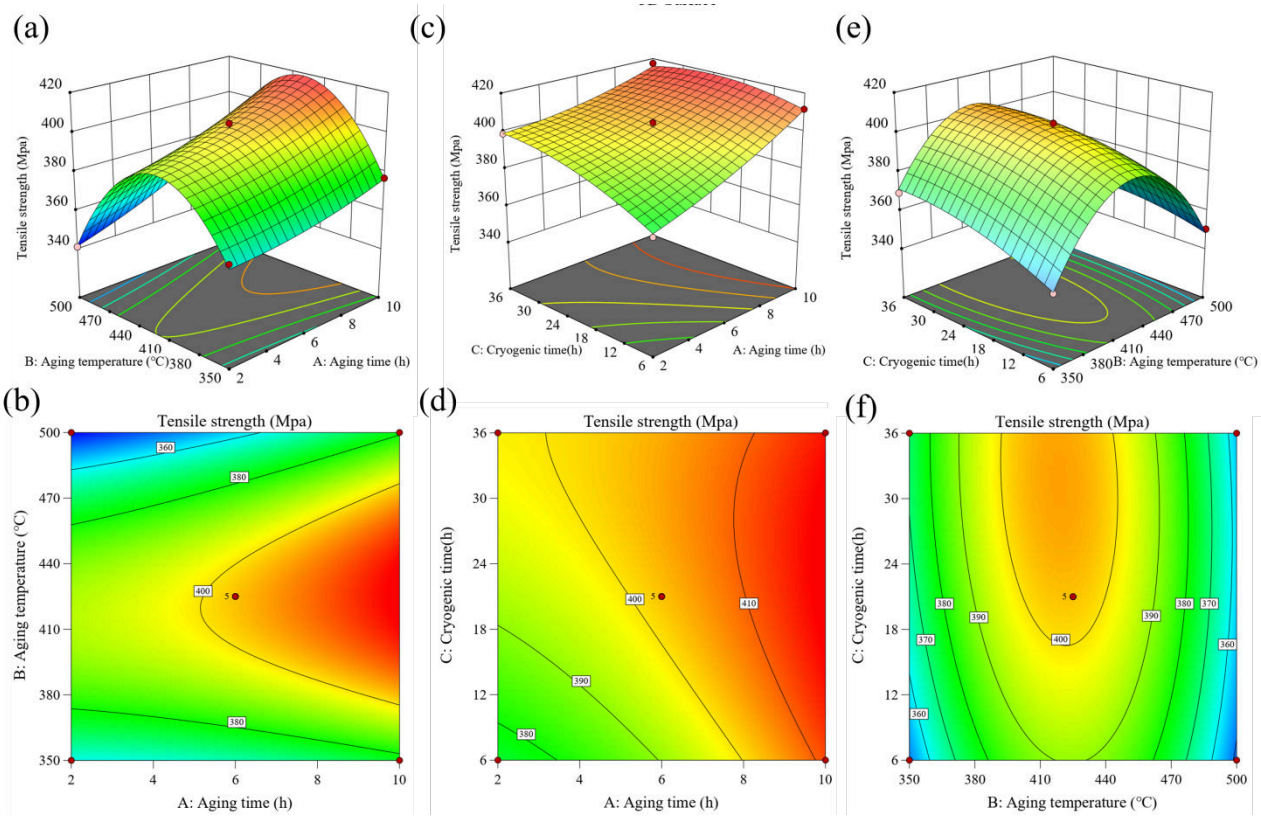


Fig. 2 3D response surface and contour lines of the influence of process parameter interaction on ultimate strength: (a), (b) aging time and aging temperature; (c), (d) aging time and cryogenic time; (e), (f) aging temperature and cryogenic time

Effects of interactions among process parameters on the elongation were manifested by 3D surface response and contour lines, as shown in Fig.3. Fig.3(a-b) shows the response surface of the interaction influence of aging temperature and aging time on the elongation. The curvature of the surface is obvious, and the curvature change in the B direction is larger than that in the A direction, indicating that the aging temperature has a greater influence on the elongation in the interaction between aging temperature and time. With the increase of aging time, the elongation decreases first, then increases. The elongation decreases first and then increases with the aging temperature increasing. The interaction of cryogenic time and aging time on elongation is shown in Figure 3 (c-d). The elongation of the alloy decreases with the increase of aging time. After combining with cryogenic treatment, the elongation of the alloy increases slightly and then decreases slowly with the extension of cryogenic treatment time. Figure 3 (e-f) shows the interaction between cryogenic time and aging temperature. The elongation of the alloy decreases first and then increases with the increase of aging temperature. When compounded with cryogenic treatment, the elongation increased first and then decreased.

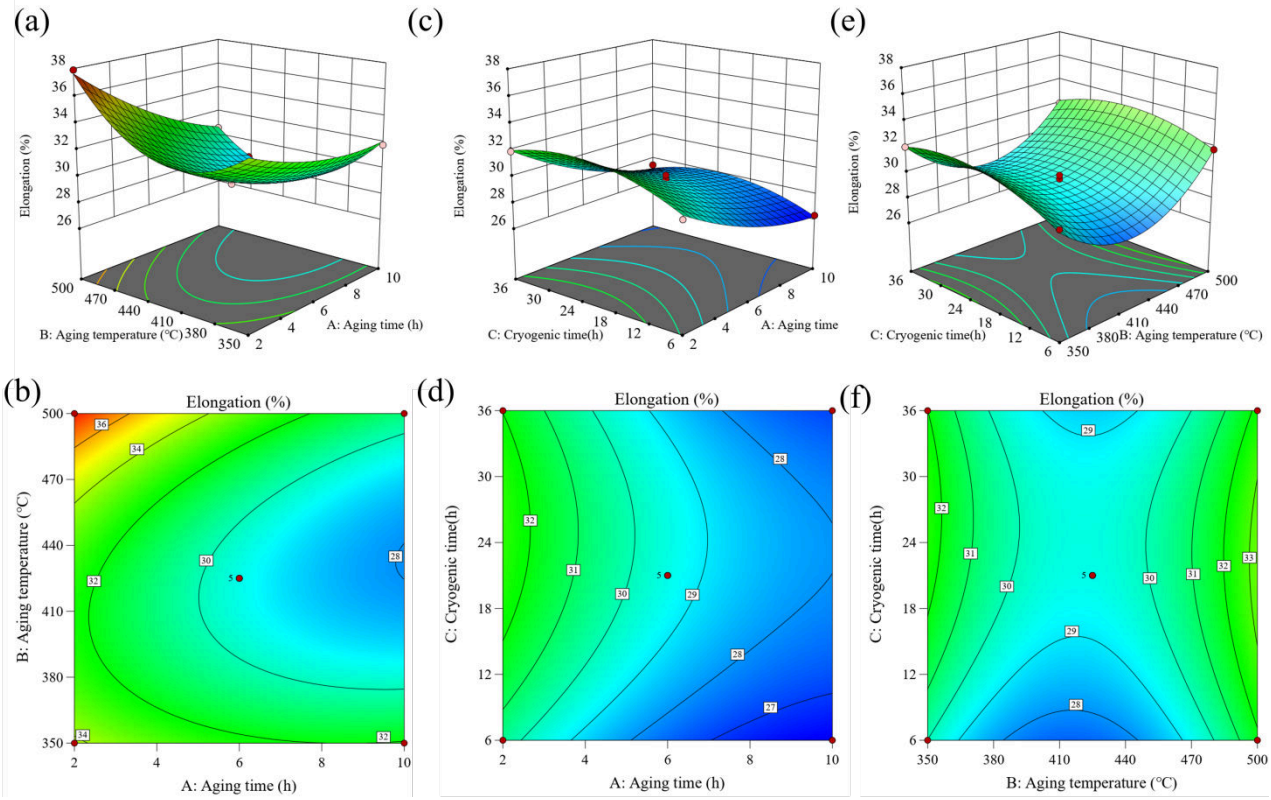


Fig. 3 3D response surface and contour lines of the influence of process parameter interaction on elongation: (a), (b) aging time and aging temperature; (c), (d) aging time and cryogenic time; (e), (f) aging temperature and cryogenic time

To sum up, the RSM solution is Cryogenic(-196℃/30h) +Aging(428℃/2h), which predicts the material could exhibit a good mechanical property.

### 3.4 Compound treatment process validation and analysis

For the purpose of confirmatory experiment, four samples were prepared with as-cast, RSM solution, best strength and worst strength obtained by different cryogenic+aging treatment parameters in actual experiment, respectively. Accordingly, the damping performance of the 4 samples were evaluated, which will be discussed in the following section. Table 5 shows the tensile properties of the samples. Appropriate cryogenic + aging treatment is beneficial to increase the tensile strength of the alloy, and the loss of elongation is controlled in a small range. Compared with the as-cast alloy, the tensile strength increased by 10.7% and the elongation decreased by 14.2% when applying the optimal parameters obtained from response surface method.

Table 5 Sample details

| Sample No. | Remark | Process parameters | Performance indicator | Experimental value |
|---|---|---|---|---|
| As-cast | As-cast | - | Elongation A/% | 38.0 |
| | | | Ultimate strength/MPa | 358.3 |
| A | Best solution by RSM | Cryogenic(-196℃/30h) +Aging(428℃/2h) | Elongation A/% | 32.6 |
| | | | Ultimate strength/MPa | 396.7 |
| B | Best strength in actual experiment | Cryogenic(-196℃/36h) +Aging(425℃/10h) | Elongation A/% | 27.4 |

| | | | | |
|---|---|---|---|---|
| | | | Ultimate strength/MPa | 417.3 |
| C | Worst strength in actual experiment | Cryogenic(-196℃/21h) +Aging(500℃/2h) | Elongation A/% | 37.9 |
| | | | Ultimate strength/MPa | 340.9 |

### 3.5 Damping properties

In order to determine the damping properties of Mn-Cu alloy after different heat treatments, the energy storage modulus and loss modulus of the alloy upon different heat treatments were measured, and the corresponding damping capacities are shown in Fig.4. In the test mode of DMA, the internal friction (IF) value of the sample ($Q^{-1}$= Tanδ) is the ratio of loss modulus to storage modulus. It can be seen that the internal friction value of the alloy is higher than 0.02 at room temperature or below, indicating that all the samples have high damping properties. The as-cast alloy has good damping properties from -50℃ to 50℃, and the best damping properties are reached at 0℃. The damping performance of sample A is significantly improved compared with that of the as-cast alloy. The range of internal friction value greater than 0.02 is increased to -100℃ to 130℃, and the peak value is 0.114. Sample B has the best strength while the highest damping performance is comparable to as-cast sample. The damping performance of sample C is increased only at low temperature, and decreases compared with the as-cast at other temperatures.

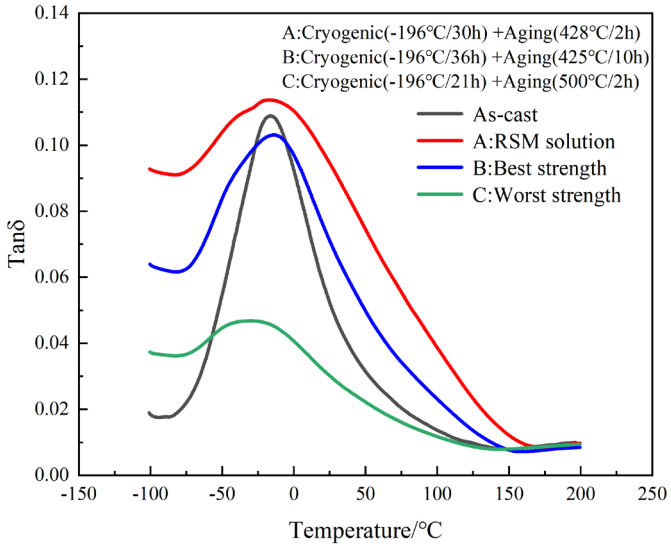


Fig. 4 Internal friction (IF) curves

Fig. 5 shows the curves of storage modulus(E) dependence of temperature. It can be seen that it shows a similar variation tendency with IF (Tanδ) dependence of temperature in the test temperature. The E value decreases firstly then increases with decrease of temperature, exhibiting a common characteristic of modulus softening caused by lattice instability owing to the paramagnetic to antiferromagnetic transition (AFT) [35]. The lattice distortion caused by antiferromagnetic order leads to lattice expansion, which weakens the binding force of atoms, so it is manifested as modulus softening. After the modulus reaches the minimum value, it gradually increases. That's because the softening effect of the modulus caused by AFT gradually weakens, and the parent phase magnetic domain twins induced by lattice distortion cause the modulus hardening [36]. It is well known that the temperature corresponding to minimum elastic modulus in E-T curve represents the martensitic transformation point of Mn-Cu based alloys [37]. The martensitic transition temperature Ms of as-cast, specimen As-cast, A, B, C are 17.61℃, 40.44℃, 24.03℃, -34.1℃, as shown in Fig. 6(a).

The temperature of martensitic transformation is closely related to the Mn content in the Mn-rich zone which is determined by the degree of spinodal decomposition [38]. It has been reported that there is a linear relationship between the martensitic transformation temperature and the Mn content in the Mn-rich region, that is, Ms (K) $=1264.8C_{Mn}-731.813$. Where Ms represents martensitic transformation temperature (K); $C_{Mn}$ is the Mn concentration (at. %) [37]. Based on the empirical equation, the $C_{Mn}$ of as-cast, A, B, and C samples are 80.8%, 82.7%, 81.4%, 76.8% respectively, as shown in Fig. 6(b). That is when treated upon cryogenic(-196℃/30h) +Aging(428℃/2h), the $C_{Mn}$ in Mn-rich region is high due to the more sufficient spinodal decomposition, thus resulting in a higher and wider phase transformation damping platform in sample A. The high fcc-fct transformation temperature promotes the formation of fct {101} twins, which improves the damping capacity of Mn-Cu based alloys.

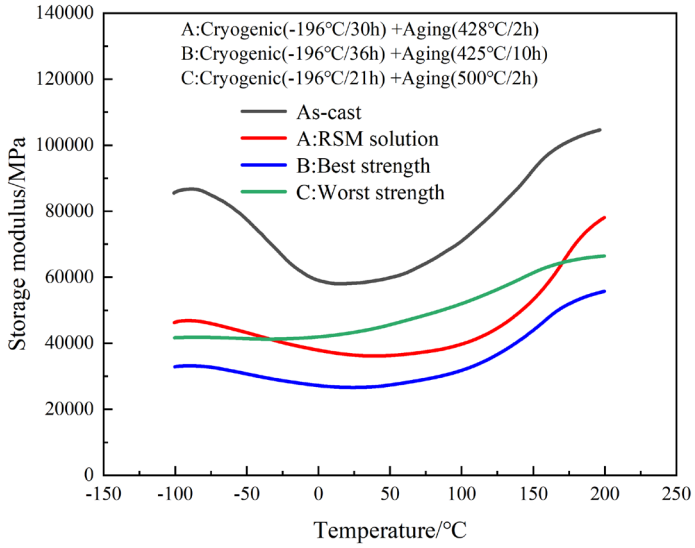


Fig. 5 Storage modulus dependence of temperature

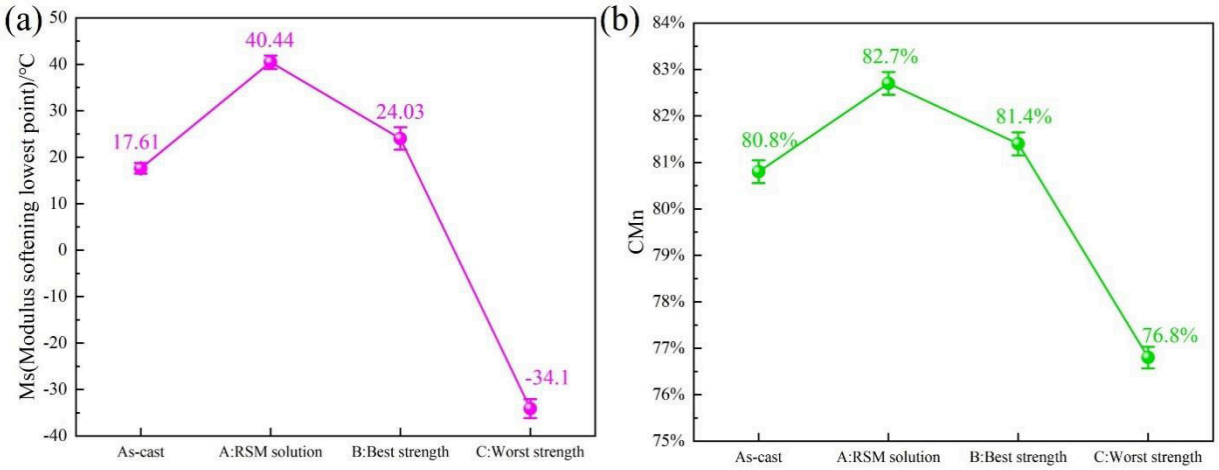


Fig. 6 (a) Martensite transformation temperature; (b) Mn content in Mn-rich region

## 4 Discussion

### 4.1 Mechanical strengthening mechanism

In general, the strength of alloys is closely related to microstructure. For further exploring the influence of cryogenic(-196℃/30h) +Aging(428℃/2h) on the mechanical and damping properties, the as-cast and specimen A

were characterized and compared. Fig. 7 shows the microstructure of as-cast sample and specimen A. The dendritical microstructures are composed of black dendrites and the surrounding bright interdendritic spacings. Compared to the as-cast sample, the dendrite size and interdendritic spacing in specimen A relatively is decreased, as shown in Fig.7(b). The grain size is finer than the as-cast sample. The reduced grain size, increasing the number of grain boundaries and hindering the dislocation movement to improve the strength of the material, as shown in Fig. 9(a).

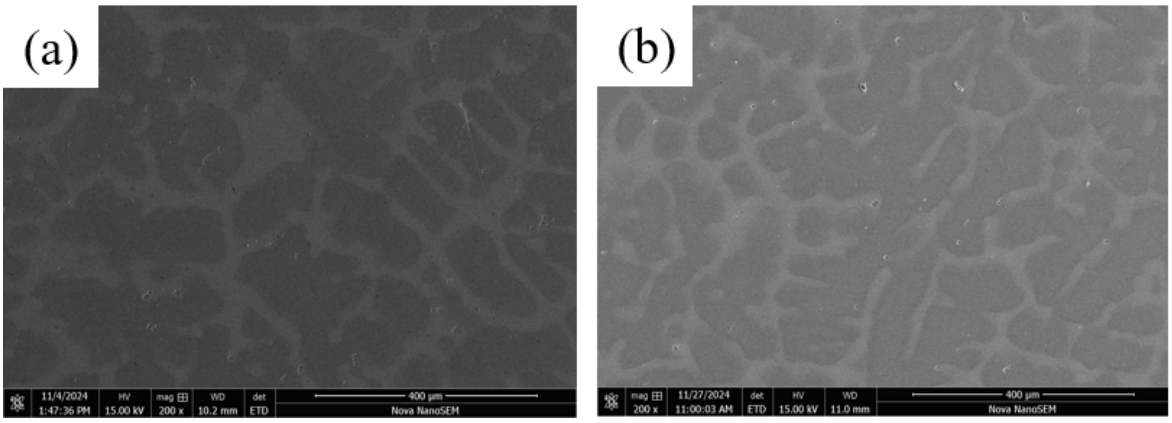


Fig. 7 Microstructure of (a) As-cast; (b) Specimen A: Cryogenic(-196℃/30h) +Aging(428℃/2h)

Fig.8 shows the XRD patterns of the as-cast and sample A, the specimen was both composed of γ phase, γ′ phase. Generally, the height of the XRD diffraction peak is related to the volume fraction of the precipitated phase. Large number of γ′ precipitates emerged in specimen A can cause cutting effect on the dislocations or impede the motion of dislocations, thus realizing precipitation strengthening and improving strength, as shown in Fig. 9(b). From Fig.11, it also indicates that many twins are formed due to martensite transformation. The twins interact with dislocation, increasing strength. At the same time, a large number of immovable total dislocations are generated at the twin boundary, which continuously slip and store to create obstacles such as dislocation entanglement, which hinders continued plastic deformation and increases the strength of the metal.

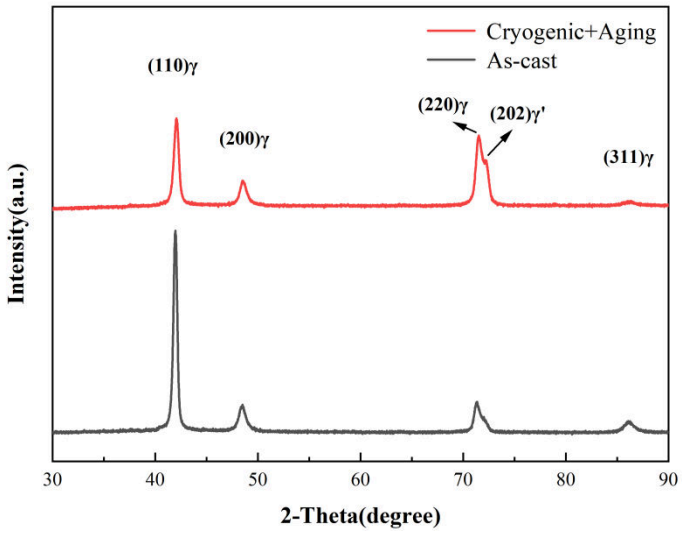


Fig. 8 XRD patterns of specimen (a) As-cast; (b) Sample A

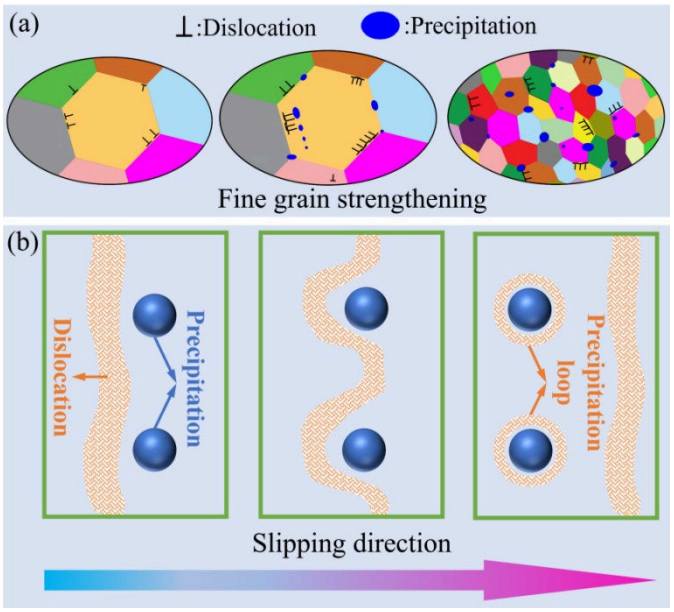


Fig. 9 Mechanical strengthening mechanisms (a) fine grain strengthening; (b) precipitation strengthening

### 4.2 Damping mechanism

Fig.10 shows the SEM images of line scan area and results on the microstructure of as-cast and specimen A. The microstructure has obvious macroscopic segregation, which is characterized by dendrite structure. The line scan results show that the dark zone is Mn-rich region, and the light zone is depleted Mn region. Furthermore, Mn is evidently predominant in the initially solidified dendritic zone compared to terminally solidified interdendritic one due to the higher melting temperature of Mn than Cu. From the EDS analysis (Fig.10(b) and 10(d)), the content of Mn in sample A is higher than that in as cast state, which indicates that the degree of Mn segregation is increased, and more Mn atoms are enriched to the primary dendrites after cryogenic(-196℃/30h) +ageing(428℃/2h) treatment. According to the open literatures [37], the fcc→fct transformation occurs firstly in Mn-rich region in the decomposition microstructure of dark dendritic zone and then in that of light interdendritic one. In other words, the two stepped fcc-fct phase transformation happens an couples to each other in the cryogenic(-196℃/30h) +aging(428℃/2h) treated Mn-Cu alloy with obvious compositional segregation, which inevitably imposes an important influence on its damping capacity, especially phase transformation damping capacity.

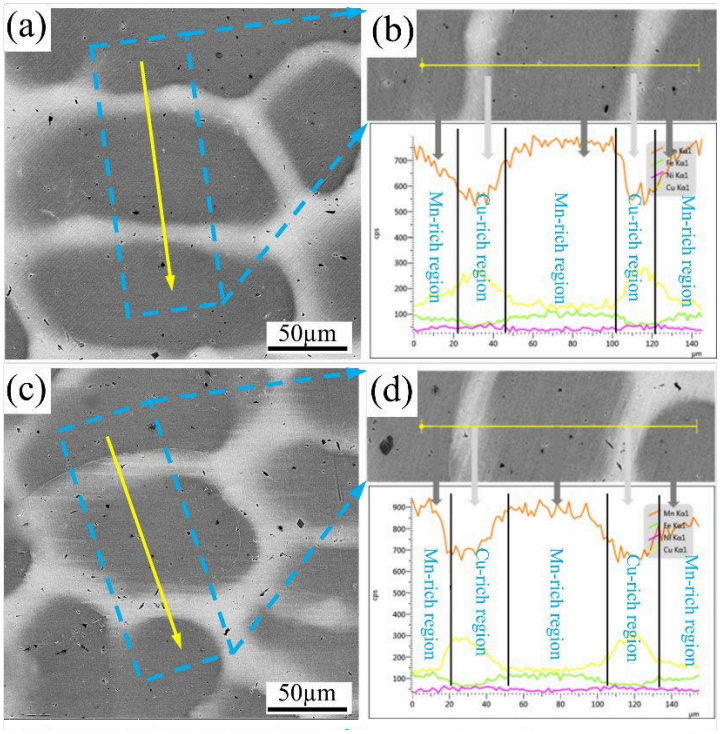


Fig. 10 SEM images of line scan area and results: (a)(b) As-cast; (c)(d) Specimen A

In addition, it can be seen from Fig.9, the original (220) diffraction peak shows obvious splitting and the diffraction peak of (202) γ′ appeared, which indicates that fcc→fct transformation occurred and {101} twins form [39] in as-cast sample and Cryogenic(-196℃/30h)+Aging(428℃/2h) treated sample. It indicates that the various axial ratios (c/a) and tetragonal distortions (1-c/a) of fct γ′-MnCu phase in the two conditioned samples. Generally, the higher 1-c/a value, i.e. larger tetragonal distortion implies more {101} twins induced by fcc-fct transformation and thus higher damping capacity of the alloy [37,24]. Fig.11 shows the EBSD images of as-cast sample and specimen A, there exhibit obvious twin bands, the twin interfaces are straight and parallel to each other, and the twins are denser in sample A [38]. It indicates that more {101} twins induced by fcc-fct transformation after cryogenic(-196℃/30h) +aging(428℃/2h) treatment. According to the study of Bacon G E and Shimizu K, the antiferromagnetic transformation and martensitic transformation of Mn–Cu alloys with high Mn content are two independent processes. Antiferromagnetic transformation is accompanied by fcc-fct structural transformation, resulting in lattice distortion and martensitic transformation induced by lattice distortion [24]. The formation of {101} twins reduce the lattice distortion caused by antiferromagnetic transformation and martensitic transformation, that is, the formation mechanism of {101} twins is stress-release induced twin mechanism. Under the action of stress, the twins will have relaxation movement, which promotes the mobility of interfaces and twin boundaries, leading to high damping capacity of the Mn-Cu based alloy. Therefore, Sample A has the best damping property within a wide temperature range.

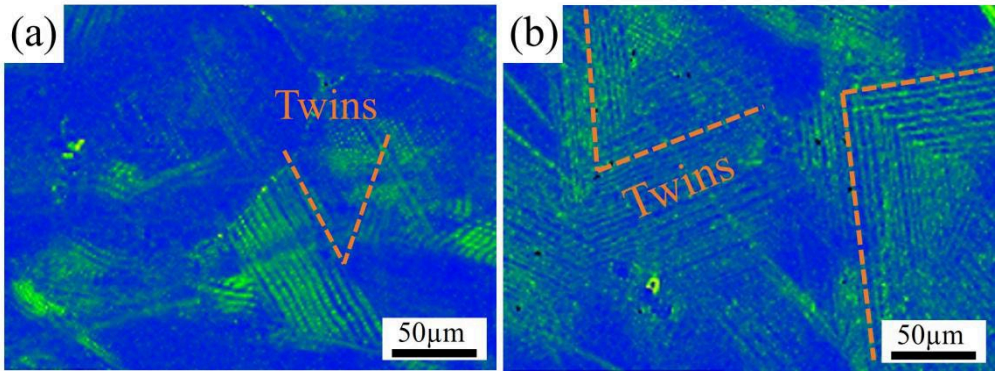

Fig. 11 EBSD images of (a) As-cast; (b) Cryogenic(-196℃/30h)+Aging(428℃/2h)

## 5 Conclusions

(1) Low temperature (-196 ℃/30h)+aging (428 ℃/2h) could effectively control the microstructure and phase composition of M2052 alloy, promoted the formation of γ 'precipitates, and improved the mechanical and damping properties of the alloy.

(2) The maximum tensile strength was 396.7MPa when the alloy treated upon Cryogenic(-196℃/30h) +Aging(428℃/2h), ~38MPa higher than as-cast alloy. This benefits from the combined effects of precipitation strengthening from the interaction of precipitates and dislocations, fine grain strengthening generated through the precipitates hindering grain growth, and twinning strengthening.

(3) When set the temperature as 50℃, the internal friction value ($Q^{-1}$) of the Cryogenic(-196℃/30h) +Aging(428℃/2h) treated alloy reached 0.074, 124% higher than the as-cast alloy. This is highly relevant to the formation of precipitates after cryogenic(-196℃/30h) + aging(428℃/2h) as well as more {101} twins induced by fcc-fct transformation.

## References


[1] L. Yang, X.S. Jiang, H.L Sun, Y.L. Zhang, Y.J. Fang, R. Shu. Synergistic enhancement in mechanical and damping properties of Cu–11Al–5Mn-0.7Ti–1Ta alloy through aging treatment. Materials Science & Engineering A 872(2023), 144925.

[2] T. Niu, H. Li, Y. Wei, Z. Zhou, Y. Liu, Novel Al-Co-Ni-Cu as-cast alloy with high damping and good corrosion resistance, J. Alloys Compd. 910 (2022), 164942, https://doi.org/10.1016/j.jallcom.2022.164942.

[3] S. S, J. Kt, K. R, A. S, Effect of Ni and Mn additions on the damping characteristics of Cu-Al-Fe based high temperature shape memory alloys, J. Alloys Compd. 924 (2022), 166258, https://doi.org/10.1016/j.jallcom.2022.166258.

[4] L. Yang, X. Jiang, H. Sun, Z. Shao, Y. Fang, R. Shu, Effect of Ta addition on microstructures, mechanical and damping properties of Cu–Al–Mn–Ti alloy, J. Mater. Res. Technol. 15 (2021) 3825–3835, https://doi.org/10.1016/j. jmrt.2021.10.031.

[5] S.W. H, F.Y. Qin, J.Y. Han, W.L. Xiao, F.S. Lu, X.Q. Zhao. Strain glass transition in high damping Mn-22Cu-5Ni-2Fe alloy. Progress in Natural Science: Materials International. 28 (2018),614-617.

[6] F.S. Lu, B. Wu, Z.F. Zhang, P. Ling, D.L. Zhao, Rare Metal. (2016).

[7] A. Agrawal, R.K. Dube, Methods of fabricating Cu-Al-Ni shape memory alloys, J. Alloys Compd. 750 (2018) 235–247, https://doi.org/10.1016/j. jallcom.2018.03.390.

[8] Y. Sutou, T. Omori, J.J. Wang, R. Kainuma, K. Ishida, Characteristics of Cu–Al–Mn-based shape memory alloys and their applications, Mater. Sci. Eng. 378 (1–2) (2004) 278–282, https://doi.org/10.1016/j.msea.2003.12.048.

[9] S.H. Chang, Influence of chemical composition on the damping characteristics of Cu–Al–Ni shape memory alloys, Mater. Chem. Phys. 125 (3) (2011) 358–363, https://doi.org/10.1016/j.matchemphys.2010.09.077.

[10] Z. Xiao, Z. Li, M. Fang, S. Xiong, X. Sheng, M. Zhou, Effect of processing of mechanical alloying and powder metallurgy on microstructure and properties of Cu–Al–Ni–Mn alloy, Mater. Sci. Eng. 488 (1–2) (2008) 266–272, https://doi.org/ 10.1016/j.msea.2007.11.037.

[11] S.K. Vajpai, R.K. Dube, S. Sangal, Microstructure and properties of Cu–Al–Ni shape memory alloy strips prepared via hot densification rolling of argon atomized powder performs, Mater. Sci. Eng., A 529 (2011) 378–387.

[12] J. Yang, Q.Z. Wang, F.X. Yin, C.X. Cui, P.G. Ji, B. Li, Effects of grain refinement on the structure and properties of a CuAlMn shape memory alloy, Mater. Sci. Eng., A 664 (2016) 215–220.

[13] A. Al´es, F. Lanzini, Mechanical and thermodynamical properties of β- Cu-Al - Mn alloys along the Cu3Al →Cu2AlMn compositional line, Solid State Commun. 319 (2020), 113980.

[14] Y. Liu, X. Xie, Z. Liu, Q. Yu, Q. Jia, S. Wang, Z. Zhang, R. Yang, R.O. Ritchie, A strong, lightweight, and damping cermet material with a nacre-like ultrafine 3D interpenetrated architecture, Mater. Today (2022), https://doi.org/10.1016/j. mattod.2022.12.002.

[15] Q. Wang, F. Han, C. Cui, Effect of heat treatment on the two internal friction peaks in a Cu–Al–Mn shape memory alloy, J. Alloys Compd. 492 (1–2) (2010) 286–290, https://doi.org/10.1016/j.jallcom.2009.11.072.

[16] A.T. Adorno, R.A.G. Silva, Ageing behavior in the Cu–10wt.%Al and Cu–10wt.% Al–4wt.%Ag alloys, J. Alloys Compd. 473 (1–2) (2009) 139–144, https://doi.org/ 10.1016/j.jallcom.2008.05.072.

[17] M. Li, J. liu, S. Yan, W. Yan, B. Shi, Effect of aging treatment on damping capacity in Cu–Al–Mn shape memory alloy, J. Alloys Compd. 821 (2020), 153213, https:// doi.org/10.1016/j.jallcom.2019.153213.

[18] K. Tsuchiya, H. Sato, S. Edo, K. Marukawa, M. Umemoto, Mater. Sci. Eng. A 285(2000) 353–356.

[19] Y.Q. Wu, F.X. Yin, K. Hono, Scr. Mater. 46 (2002) 717–722.

[20] Y. Zhong, T. Sakaguchi, F.X. Yin, Mater. Sci. Eng. A 492 (2008) 419–427.

[21] X.Q. Zhao, Y. Liang, Q.H. Zhuang, B.X. Liu, Jpn. J. Appl. Phys. 35 (1996)4468–4473.

[22] L.P. Wang, E.J. Guo, X.R. Yao, X.S. Zhu, Crystal structure changes of Mn-Cu damping alloy at aging. The Chinese Journal of Nonferrous Metals.13(1):46-50.

[23] W. Li, Q.F. Li, X.L. Zhang, Y.Q. Sun, H.J. Zhao, Z.B. Liu. Remarkable improvement in damping capacity of M2052 alloy by step-cooling treatment by step-cooling treatment, J. Mater. Res. Express 8 (2021) 016526.

[24] S.N. Saud, E. Hamzah, T. Abubakar, H.R. Bakhsheshi-Rad, S. Farahany, A. Abdolahi, M.M. Taheri, Influence of Silver nanoparticles addition on the phase transformation, mechanical properties and corrosion behaviour of Cu–Al–Ni shape memory

alloys, J. Alloys Compd. 612 (2014) 471–478, https://doi.org/10.1016/j. jallcom.2014.05.173.

[25] Q. Zhang, B. Cui, B. Sun, X. Zhang, Z. Dong, Q. Liu, T. Cui, Effect of Sm doping on the microstructure, mechanical properties and shape memory effect of Cu-13.0Al- 4.0Ni alloy, Materials 14 (14) (2021), 144007, https://doi.org/10.3390/ ma14144007.

[26] X. Zhang, T. Cui, X. Zhang, Q. Liu, Z. Dong, C. Man, Effect of Nd addition on the microstructure, mechanical properties, shape memory effect and corrosion behaviour of Cu–Al–Ni high-temperature shape memory alloys, J. Alloys Compd. 858 (2021), 157685, https://doi.org/10.1016/j.jallcom.2020.157685.

[27] X. Zhang, J. Sui, Q. Liu, W. Cai, Effects of Gd addition on the microstructure, mechanical properties and shape memory effect of polycrystalline Cu-Al-Ni shape memory alloy, Mater. Lett. 180 (2016) 223–227, https://doi.org/10.1016/j. matlet.2016.05.149.

[28] S.N. Saud, E. Hamzah, H.R. Bakhsheshi-Rad, T. Abubakar, Effect of Ta additions on the microstructure, damping, and shape memory behaviour of prealloyed Cu-Al-Ni shape memory alloys, Scanning (2017), 1789454, https://doi.org/10.1155/2017/ 1789454, 2017.

[29] F.X. Yin, Kotobu Nagai, Kenji Watanabe and Kohji Kawahara. The Damping Behavior of Ni Added Mn–Cu Damping Alloys. Materials Transactions, Vol. 44, No. 9 (2003) 1671-1674.

[30] D.W. Wang, H.k. Niu, S.B. Zhang, W.D. Xuan, Z.M. Ren, Q.C. Tian. Enhancement of Damping Capbility of MnCu Alloy by High Magnetic Field. Metals 2023, 13, 6.

[31] G Li, H Wang, X.P. Wang, Y.X. Gao, W.B. Jiang, Q.F. Fang. Preparation and properties of novel Mn-27Cu porous alloy with a low density and high damping capacity. Nonferrous metals engineering. Vol.10, No.5 (2020):1-5.

[32] D chen, J.F. Dong, G.Z. Ma, et al. The research about cryogenic treatment process of nonferrous alloys- a review[J]. Materials Reports, 2010, 24(21): 1-4.

[33] H.K. Cai, Z.J.Weng, K.X.Gu, et al. Advances in deep cryogenic treatment of cemented carbide[J]. Materials Reports, 2019, 33(1): 175-182.

[34] W.H. Liu, L.N. Li, H. Huang, et al. Effect of cryogenic treatment on microstructure and mechanical properties of 7A62 aluminum alloy[J]. The Chinese Journal of Nonferrous Metals. DOI: 10.11817/j.ysxb.1004.0609.2023-44634.

[35] S.B. Zhang. Parent-phase twinning induced ultra-high damping capacity of Mn–20Cu–5Ni–2Fe alloy under directional solidification process[J]. Intermetallics. 138(2021)107343.

[36] C.H. Ma. Research on forming M2052 manganese copper alloy and its post-treatment technology based on SLM technology[D]. Kunming University of Science and Technology. 2020.

[37] S Zhang, X.P. Guo, Y Tang, S Zhong, Y.G. Xu. A comparative study on microstructure and damping capacity of Mn-Cu based alloys with dendrite and equiaxial grain. Vacuum 168 (2019) 108814.

[38] Q.F. Li. Study on heat treatment process and microstructure and properties of as cast Mn-19Cu-5Ni-2Fe damping alloy[D]. Jiangxi University of Science and Technology. 2020.

[39] F. Yin, Y. Ohsawa, A. Sato, K. Kawahara, X-ray diffraction characterization of the decomposition behavior of γ-Mn phase in a Mn-30 at.% Cu alloy, Scr. Mater. 40 (9) (1999) 993–998.

https://dspace.org/

# Effect of the combined use of cryogenic + aging treatment on mechanical and damping property of Mn-Cu alloy based on response surface model

**Ding, Ran; Liu, Guang-lei; Liu, Shu-cong; Ranjbar, Mostafa; Potter, Andrew ...**

**2025-06-01**
Elsevier
https://doi.org/10.1016/j.mtcomm.2025.112655
Ding R, Liu G-L, Liu S-C, et al., (2025) Effect of the combined use of cryogenic + aging treatment on mechanical and damping property of Mn-Cu alloy based on response surface model. Materials Today Communications, Volume 46, June 2025, Article number 112655

Downloaded from a DSpace repository. https://dspace.org/